**Revision_1**

# H-bonding scheme and cation partitioning in axinite: A single-crystal neutron diffraction and Mössbauer spectroscopic study

**G. Diego Gatta[1,2], Günther J. Redhammer[3], Alessandro Guastoni[4], Giorgio Guastella[5], Martin Meven[6], Alessandro Pavese[1]**

[1] Dipartimento di Scienze della Terra, Università degli Studi di Milano, Via Botticelli 23, I-20133 Milano, Italy
[2]CNR - Istituto di Cristallografia, Via G. Amendola 122/o, Bari, Italy
[3]Abteilung für Materialwissenscgaften & Mineralogie, Fachbereich Chemie und Physik der Materalien, Universität Salzburg, Austria
[4] Dipartimento di Geoscienze, Università degli Studi di Padova, Via Gradenigo 6, I-35131 Padova, Italy
[5]Agenzia delle Dogane e dei Monopoli, Direzione Regionale per la Lombardia, Laboratorio e Servizi Chimici, Via Marco Bruto 14, I-20138 Milano, Italy
[6]Institut für Kristallographie, RWTH Aachen, and Jülich Centre for Neutron Science (JCNS) at Heinz Maier-Leibnitz Zentrum (MLZ), Lichtenbergstraße 1, D-85748 Garching, Germany

**Running title:** Crystal chemistry of ferroaxinite



**Corresponding author: G. Diego GATTA**

Dip. Scienze della Terra
Universita' degli Studi di Milano
Via Botticelli, 23
I-20133 Milano, Italy
Tel. +39 02 503 15607
Fax +39 02 503 15597
E-Mail: diego.gatta@unimi.it

(To be submitted to *Physics and Chemistry of Minerals*)

# H-bonding scheme and cation partitioning in axinite: A single-crystal neutron diffraction and Mössbauer spectroscopic study

**G. Diego Gatta[1,2], Günther J. Redhammer[3], Alessandro Guastoni[4], Giorgio Guastella[5], Martin Meven[6], Alessandro Pavese[1]**

[1] Dipartimento di Scienze della Terra, Università degli Studi di Milano, Via Botticelli 23, I-20133 Milano, Italy
[2]CNR - Istituto di Cristallografia, Via G. Amendola 122/o, Bari, Italy
[3]Abteilung für Mineralogie, FB Materialforschung & Physik, Universität Salzburg, Hellbrunnerstr. 34/III, 5020 Salzburg, Austria
[4] Dipartimento di Geoscienze, Università degli Studi di Padova, Via Gradenigo 6, I-35131 Padova, Italy
[5]Agenzia delle Dogane e dei Monopoli, Direzione Regionale per la Lombardia, Laboratorio e Servizi Chimici, Via Marco Bruto 14, I-20138 Milano, Italy
[6]Institut für Kristallographie, RWTH Aachen, and Jülich Centre for Neutron Science (JCNS) at Heinz Maier-Leibnitz Zentrum (MLZ), Lichtenbergstraße 1, D-85748 Garching, Germany

## Abstract

The crystal chemistry of a ferroaxinite from Colebrook Hill, Rosebery district, Tasmania, Australia, was investigated by electron microprobe analysis in wavelength-dispersive mode, inductively coupled plasma-atomic emission spectroscopy (ICP-AES), $^{57}$Fe Mössbauer spectroscopy, and single-crystal neutron diffraction at 293 K. The chemical formula obtained on the basis of the ICP-AES data is the following:

$^{X1,X2}Ca_{4.03}{}^{Y}(Mn_{0.42}Mg_{0.23}Fe^{2+}_{1.39})_{\Sigma 2.04}{}^{Z1,Z2}(Fe^{3+}_{0.15}Al_{3.55}Ti_{0.12})_{\Sigma 3.82}{}^{T1;T2,T3,T4}(Ti_{0.03}Si_{7.97})_{\Sigma 8}{}^{T5}B_{1.96}O_{30}(OH)_{2.18}$.

The $^{57}$Fe Mössbauer spectrum shows unambiguously the occurrence of $Fe^{2+}$ and $Fe^{3+}$ in octahedral coordination only, with $Fe^{2+}/Fe^{3+}$ = 9:1. The neutron structure refinement provides a structure model in general agreement with the previous experimental findings: the tetrahedral *T1*, *T2*, *T3* and *T4* sites are fully occupied by Si, whereas the *T5* site is fully occupied by B, with no evidence of Si at the *T5*, or Al or $Fe^{3+}$ at the *T1*-*T5* sites. The structural and chemical data of this study suggest that the amount of B in ferroaxinite is that expected from the ideal stoichiometry: 2 *a.p.f.u.* (for 32 O). The atomic distribution among the *X1*, *X2*, *Y*, *Z1* and *Z2* sites obtained by neutron structure refinement is in good agreement with that based on the ICP-AES data. For the first time, an unambiguous localization of the H site is obtained, which forms a hydroxyl group with the oxygen atom at the *O16* site as *donor*. The H-bonding scheme in axinite structure is now fully described: the *O16*-*H* distance (corrected for riding motion effect) is 0.991(1) Å and an asymmetric bifurcated bonding configuration occurs, with *O5* and *O13* as *acceptors* (*i.e.*, with *O16*···*O5* = 3.096(1) Å, *H*···*O5* = 2.450(1) Å and *O16*-*H*···*O5* = 123.9(1)°; *O16*···*O13* = 2.777(1) Å, *H*···*O13* = 1.914(1) Å and *O16*-*H*···*O13* = 146.9(1)°).

**Keywords:** axinite; single-crystal neutron diffraction; Mössbauer spectroscopy; H-bonding scheme; cation partitioning.

## Introduction

The axinite-group minerals are chemically (and structurally) complex borosilicates with general formula $(Ca,Mn)_4(Mn,Fe,Mg)_2Al_4B_2Si_8O_{30}(OH)_2$. Axinites typically occur in low- to medium-grade metamorphic environments, in particular in Ca- and B-rich (but relatively Al-poor) environments, and the different *P-T-X-*$f_{O2}$ conditions govern the remarkable compositional variability of this mineral group (Pringle and Kawachi 1980; Grew 1996).

Axinite often occurs in large crystals (mm- to cm-sized), which have a relatively good hardness (ranging from 6.5 - 7 on the Mohs scale). One of the main uses of axinite is in the jewelry market, because it is one of the few gemstones that possess a strong pleochroism and high brilliance (*i.e.*, cut crystals are usually intensely trichroic, with the brown and purple colors dominating; birefringence 0.010-0.012), well appreciated features for a jewel. Crystals of axinite are transparent to translucent, and have a distinctively strong vitreous luster when cut and polished. Cut and clear axinite larger than 5 carats are very rare. The ability to fix up the provenance of a gem-quality axinite stock, through a detailed cystal-chemistry characterization of some of its samples, is a key-point to provide a correct economic assessment of such a material on the gemstones market.

The first structure model of axinite was reported by Ito and Takéuchi (1952) and later revised by Ito et al. (1969) and Takéuchi et al. (1974, 1975), in the space group *P*-1 with $a \sim 7.16$ Å, $b \sim 9.20$ Å, $c \sim 8.97$ Å, $\alpha \sim 91.8°$, $\beta \sim 98.1°$, and $\gamma \sim 77.2°$. Structural investigations of different members of the axinite group were successively reported by several authors (*e.g.*, Swinnea et al. 1981; Belokoneva et al. 1997, 2001; Andreozzi et al. 2000a, 2000b, 2004; Filip et al. 2006). The topology of the axinite structure is complex. The structure is built up by a sequence of alternating sheets of tetrahedra and octahedra, as shown in Fig. 1. In the tetrahedral sheets, there are two different building units: *a)* two disilicate groups are connected by two B-tetrahedra to form a six-membered ring, *b)* two further disilicate groups share a corner with the B tetrahedra forming a complex $[B_2Si_8O_{30}]$ unit. In the octahedral sheets, edge-sharing distorted octahedra, populated by Al, Mn, Fe, or Mg, form six-membered finite chains, which are laterally connected by distorted Ca-octahedra.

A few studies were devoted to the classification of axinite group minerals (Sanero and Gottardi 1968) and to their physical properties (*e.g.*, Lumpkin and Ribbe 1979; Filip et al. 2008). Andreozzi et al. (2004) proposed a new crystal-chemical formula for the axinite mineral group: $^{VI}[X1\ X2\ Y\ Z1\ Z2]_2\ ^{IV}[T1\ T2\ T3\ T4\ T5]_2O_{30}(OwOH_{1-w})_2$,

where VI and IV are coordination numbers; *X1* = Ca and very minor Na; *X2* = Ca (in axinites) or Mn (in tinzenite); *Y* = Mn (in manganaxinite and tinzenite), $Fe^{2+}$ (in ferroaxinite) or Mg (in magnesioaxinite), with minor Al and $Fe^{3+}$; *Z1* = Al and $Fe^{3+}$; *Z2* = Al; *T1*, *T2*, and *T3* = Si; *T4* = Si (and presumably very minor B); *T5* = B and minor Si. Charge unbalance (*w*), due to heterovalent substitutions, is compensated for by $O^{2-} \rightarrow OH^{-}$ substitution.

The structural refinements of different members of the axinite group were all based on X-ray diffraction data (*e.g.*, Takéuchi et al. 1974; Swinnea et al. 1981; Belokoneva et al. 1997, 2001; Andreozzi et al. 2000a, 2000b, 2004; Filip et al. 2006). On the basis of literature data, a poorly defined picture of the configuration of the O-H groups and of the H-bonding scheme still exists. Andreozzi et al. (2000a) studied the crystal chemistry of 60 samples of axinites from 24 worldwide localities by single-crystal X-ray diffraction, electron and ion microprobe, and $^{57}Fe$ Mössbauer spectroscopy. These authors showed evidence that B (instead of Al) is inversely related with Si, and that $Fe^{3+}$ is the main substitute for Al, but also for divalent cations, and that these heterovalent substitutions are balanced by an OH deficiency. Moreover, Andreozzi et al. (2004) highlighted how Fe partitioning among octahedral and/or tetrahedral sites must be defined for a reliable description of the crystal chemistry of axinites. Iron in axinite is reported to occur both in the divalent and in the trivalent valence state. Quantification of the $Fe^{3+}/Fe^{2+}$ ratio is reliably done using $^{57}Fe$ Mössbauer spectroscopy, which also allows one, on the basis of the hyperfine parameters, to discern between octahedral and tetrahedral coordination. This method was applied several times to study axinite, among others by Pieczka and Kraczka (1994), Fuchs et al. (1997), Andreozzi et al. (2000a, 2000b, 2004), Novak and Filip (2002), Zabinski et al. (2002), and Filip et al. (2006). Most of these studies show that $Fe^{2+}$ is dominating in ferro- and magnesioaxinite, and in this condition one single doublet is sufficient to model the $Fe^{2+}$ resonance absorption contribution. In contrast, $Fe^{3+}$ is the dominant form or iron in manganaxinite and tinzenite (Filip et al. 2008). Following Andreozzi et al. (2004), $Fe^{2+}$ populates the *Y* site. For $Fe^{3+}$ some contradicting interpretations are found. Fuchs et al. (1997) attributed it to the tetrahedral site (even if isomer shift values would be unduly large for $Fe^{3+}$ in tetrahedral coordination), whereas, according to a more shared opinion, $Fe^{3+}$ is supposed to enter the octahedral sites (especially the *Z1* site and to a lesser extent the *Y* site, Andreozzi et al. 2004, Filip et al. 2006).

The present study re-investigates the crystal structure and crystal chemistry of an axinite from Colebrook Hill, Rosebery district, Tasmania, Australia, with the aim to provide a reliable location of the proton site for a full description of the atomic relationship via the H bond. To achieve this goal and obtain a clear picture of cations ordering at the tetrahedral and octahedral sites, we used electron microprobe analysis in wavelength-dispersive mode (EPMA-WDS), inductively coupled

plasma-atomic emission spectroscopy (ICP-AES), $^{57}$Fe Mössbauer spectroscopy, and single-crystal neutron diffraction (SCND). This investigation is the latest in a series of single-crystal neutron diffraction experiments that we have recently devoted to hydrous B-bearing minerals (*e.g.*, Gatta et al. 2010, 2012a, 2012b, 2014a).

## Sample description and mineralogy

We have selected a sample of axinite from Colebrook Hill, Rosebery district, Tasmania, Australia, provided by the Museum of Mineralogy of the University of Padova (Italy), ref. MMP M13333. The sample utilized for this study contains large laminar, brown crystals of axinite up to several millimetres in length, lined in a cavity associated with quartz crystals, dissolved from the enclosing calcite with acids. The rock matrix is composed by an aggregate of microcrystalline axinite and green diopside. Back-scattered images obtained on a polished section of axinite-(Fe) (collected by a scanning electron microprobe) have shown diffused micrometric inclusions of titanite as well.

Colebrook Hill mine has produced Australia's best axinite specimens (ferroaxinite), some of which are world class. The deposit is hosted by an unusual skarn, sometimes described as a limurite or axinite-hornfels, probably derived from calcareous or dolomitic rocks associated with mafic-ultramafic intrusive rocks, these latter formed by sills and dykes of serpentinized pyroxenite and gabbro (Blisset 1962). The skarn is supposed to derive from boron and sulphur-rich reactive hydrothermal solutions from an underlying granite of Devonian age.

Colebrook Hill mine was originally quarried for copper; indeed the most abundant mineral is ferroaxinite. The main metallic minerals are pyrrhotite, pyrite, chalcopyrite and arsenopyrite. Small amounts of marcasite, galena, sphalerite and tetrahedrite were also observed. Additional boron-bearing silicates, represented by datolite and danburite, occur in vugs as well, but are rare. Gangue minerals are common and formed by calcite and quartz. Banded ore consists of alternating bands of axinite, actinolite and diopside. Much of the sulphides, calcite and quartz are associated with the axinite, with crystals up to 2-3 centimetres in length lined in the cavities filled with calcite. The sulphides usually occur as irregular patches throughout the axinite veins, or in bands between the axinite and the actinolite veins. The massive ore is made of crystals of ferroaxinite, actinolite, diopside, calcite and quartz. The sulphides, in particular pyrrhotite and chalcopyrite, occur either disseminated through the ore or as irregular veins (Petterd 1910; Blisset 1962)

## Experimental methods:

### 1)_Chemical analyses

Scanning electron microscope observations were performed using a SEM JEOL-5610 LV at the Museum of Natural History of Milan, Italy. Chemical composition of ferroaxinite was obtained by a CAMECA SX-50 electron microprobe equipped with four wavelength dispersive spectrometers and one energy dispersive spectrometer at the laboratory of microanalysis of the Institute for Geosciences and Earth Resources of CNR (Padova, Italy). The operating conditions were 20 kV accelerating voltage and 20 nA beam current. Counting times were 10 s at the peak and 5 s at the background for major elements Mg, Al, Si, Ca, Mn and Fe. Emission X-ray counts were converted into oxide weight percentages using the PAP correction program (Pouchou and Pichoir 1985). Crystals were found to be chemically homogeneous within the analytical error. The chemical formula, obtained by averaging 20-point analyses, is given in Table 1.

A total mass of 762 mg of the axinite sample was used for the ICP-AES chemical analyses. Sample preparation, standardization, quantification of uncertainty in measurement and analytical methods were performed using the guidelines of the following international protocols: EN ISO 21587 (2007) (parts 1, 2 and 3), 26845 (2008), 21078 part 1 (2008); EPA 3052 (1996), 6010c (2007), 9214 (1996); JGCM 100 (2008); as reported by Gatta et al. (2014b). Sample preparation was carried out in two ways:

1) Microwave assisted acid attack at 200°C with a mixture of sulfuric acid, hydrochloric acid and hydrofluoric acid; subsequent complexation of fluorides with boric acid;

2) Decomposition by alkaline fusion with sodium carbonate, potassium carbonate or mixture of sodium carbonate and boric acid, in a muffle furnace at 1000-1100°C for 15 minutes. Subsequent removal of silica by means of hydrofluoric acid and dissolution in mixture of hydrochloric acid and sulfuric acid.

Major elements, as Si and Al, were determined by at least two different methods: Si content was determined by gravimetrical method and ICP-AES; Al content was determined by ICP-AES and volumetric method, with separation by cupferron with addition of CyDTA in excess and retro-titration with zinc standard solution. B was measured by means of ICP-AES. Ca, Fe, Mn and other minor elements were determined by ICP-AES on aqueous solutions resulting from acid attack and alkaline fusion. Several analytical standard solutions were used to make a calibration curve, and various certified material standards were used as analytical control. Weight determination was carried out by means of an Analytical Balance GENIUS – Sartorius ME235P. A Berghof speedwave 4 apparatus was used as microwave digestion system. ICP-AES chemical analyses were performed by a Perkin Elmer Optima 7000 DV spectrometer. In this apparatus, the sample-

introduction unit includes a cyclonic spray chamber and a MEINHARD-type concentric glass nebulizer. The cyclonic spray chamber was used to provide both high sample transfer into the ICP and fast sample rinse-in and rinse-out times. The concentric nebulizer provided excellent sensitivity and precision for aqueous solutions. The final chemical composition of the axinite, along with further details pertaining to the analytical methods, is given in Table 2.

**2)_Single-crystal neutron diffraction experiment**

Single crystals of axinite, optically free of inclusions or fractures under a transmitted-light polarizing microscope, were selected for the diffraction experiments. The unit-cell parameters at room temperature were first measured by single-crystal X-ray diffraction (using a small crystal 0.28 x 0.18 x 0.12 mm) with an Oxford Diffraction four-circle diffractometer equipped with a CCD, at the Earth Sciences Dept., University of Milan (Italy). A total of 1980 reflections were measured, giving a metrically triclinic unit-cell with: $a$ = 7.1629(2) Å, $b$ = 9.2019(3) Å, $c$ = 8.9608(3) Å, $\alpha$ = 91.792(2)°, $\beta$ = 96.66(4)°, $\gamma$ = 77.307(3)°, and $V$ = 570.26(3) Å$^3$ (Table 3).

A suite of crystals was sorted out for the neutron diffraction experiment. The diffraction patterns showed that mosaicity affects all the crystals of the axinite sample used in this study. A monochromatic single-crystal neutron diffraction experiment was performed on a crystal of axinite (3.2 x 3.1 x 2.5 mm) using the hot source (fast neutrons) diffractometer HEiDi at the neutron source FRM II of the Heinz Maier-Leibnitz-Zentrum (MLZ), Germany. A first set of diffraction data were collected at 293 K, with a wavelength of the incident beam of 1.170(1) Å up to $2\theta_{max}$ =124° ($\sin(\theta)/\lambda$ = 0.75 Å$^{-1}$) [Ge-311 monochromator, Er foil filter to suppress $\lambda/3$ contamination]. A $^3$He single counter detector was used. The unit-cell parameters were refined on the basis of the 28 Bragg reflections, confirming a triclinic lattice, as previously observed by X-ray data (Table 3). A second set of intensity data were collected at higher $\sin(\theta)/\lambda$ up to 0.89 Å$^{-1}$ with a wavelength of the incident beam of 0.7925(5) Å, focusing on those reflections for which significant intensity could be expected from preliminary results of the first data set. A total of 6525 reflections were collected up to $d_{min}$ = 0.56 Å (with $-12 \le h \le +12$, $-16 \le k \le +16$ and $-16 \le l \le +16$, Table 3), using pure $\omega$-scan, $\omega$-$2\theta$ scan and $\omega$-$2\theta$ scan strategy (Table 3), out of which 5440 with $F_O > 4\sigma(F_O)$ (Table 3). Integrated intensities were then corrected for the Lorentz effect; absorption correction was found to be negligible. Further details pertaining to the data collection are reported in Table 3.

**3)_Mössbauer spectroscopy**

Transmission $^{57}$Fe Mössbauer spectra were collected at room temperature using a Mössbauer apparatus (HALDER electronics, Germany) in horizontal arrangement ($^{57}$Co/Rh single line thin source, constant acceleration mode, symmetric triangular velocity shape, multi-channel analyser with 1024 channels, velocity scale calibrated to α-iron). For Mössbauer absorber preparation, 68 mg of the sample was first ground in ethanol, then filled into Cu-rings (inner diameter 10 mm and covered with a high-purity Al-foil on one side), and mixed with epoxy resin to fix the sample. The folded spectra were analysed using classical full static Hamiltonian site analysis (using Lorentzian shaped doublets) with the program RECOIL (Rancourt and Ping 1991).

## Results: Neutron structure refinement of axinite

The neutron intensity data collected at 293 K were first processed in order to calculate the normalized structure factors (*E*'s) and their statistical distributions (using the program E-STATISTICS, implemented in the WinGX package; Farrugia 1999). The structure was found to be centrosymmetric (with 89% likelihood; $|E^2-1| = 0.913$). The anisotropic structure refinement was then performed in the space group *P*-1 using the SHELX-97 software (Sheldrick 1997, 2008), starting from the (H-free) structure model of Andreozzi et al. (2004). The neutron scattering lengths of Ca, Mn, Fe, Al, B, Si, O, and H were used according to Sears (1986). The effects of secondary isotropic extinction were corrected following the Larson's formalism (Larson 1967), as implemented in SHELXL-97. In order to have a clear picture of the cations distribution among the octahedral and tetrahedral sites, the first cycles of the refinement were conducted with the following protocol:

1) The *T1*, *T2*, *T3* and *T4* sites were first modelled with a mixed neutron scattering length of Si and Al, and then with Si and B. However, the potential fraction of Al or B was found being not significant (Table 4).
2) The *T5* site was modelled with a mixed (Si + B) scattering length. However, the fraction of Si was found being not significant (Table 4).
3) The *X1* and *X2* sites were first modelled with a mixed (Ca + Mn) scattering length. Only at the *X2* sites the fraction of Mn was found being significant (Table 4).
4) The *Y* site was modelled with a mixed (Mn + Fe) scattering length, and the Mn/Fe fraction was refined (Table 4).
5) The *Z1* and *Z2* sites were modelled with a mixed (Al + Fe) scattering length. Only the *Z1* site showed a significant fraction of Fe (Table 4).

6) All the oxygen sites (*i.e.*, *O1-O16*, Table 4) were modelled with scattering length of O, showing full site occupancies.

When convergence was achieved, one negative residual peaks was found in the final difference-Fourier map of the nuclear density at $x \sim -0.006$, $y \sim 1.04$, $z \sim 0.38$ (Fig. 2). The final cycles of anisotropic refinement were then conducted assigning H to this residual peaks (as hydrogen has a negative neutron scattering length), which was modelled with an anisotropic displacement regime and its site occupancy factor was refined, giving a final full occupancy within 1σ. Convergence was rapidly achieved, with no significant correlation among the refined parameters in the variance-covariance matrix. No peaks larger than -0.86/+0.87 fm/Å$^3$ were found in the final difference-Fourier map of the nuclear density at the end of the refinement (Table 3). The final agreement index $R_1(F)$ was 0.032 for 251 refined parameters and 5440 unique reflections with $Fo>4\sigma(Fo)$ (Table 3). Atomic coordinates and displacement parameters are listed in Tables 4 and 5; relevant bond lengths and angles are listed in Table 6.

## Results: Mössbauer spectrum of axinite

The $^{57}$Fe Mössbauer spectrum of axinite is shown in Fig. 3. It is dominated by a doublet with hyperfine parameters typical for $Fe^{2+}$ in octahedral coordination. There is no evidence of a second $Fe^{2+}$ doublet as found *e.g.* by Andreozzi et al. (2004) in some rare cases. A distinct shoulder at ~ 0.4 mm/s is indicative for the presence of $Fe^{3+}$; the obtained hyperfine parameters (Table 7) are typical for $Fe^{3+}$ in octahedral coordination and the relative area fraction of this component is 10.3(9) %. The width of the shoulder for $Fe^{3+}$ is small and, as for $Fe^{2+}$, no evidence is seen for a second $Fe^{3+}$ component, which would indicate that $Fe^{3+}$ is distributed over different sites. The obtained spectrum for axinite of this study and the derived $^{57}$Fe Mössbauer parameters agree very well with data previously reported in the literature (*e.g.*, Fuchs et al. 1997; Andreozzi et al. 2004; Zabinski et al. 2002; Filip et al. 2006).

## Discussion

The chemical composition of the axinite from from Colebrook Hill, Rosebery district, Tasmania, Australia, based on EPMA-WDS and ICP-AES analyses, suggests that the sample is a ferroaxinite (following Andreozzi et al. 2004). EPMA-WDS and ICP-AES data are mutually consistent. The ICP-AES data are considered as the reference ones, and the recalculation of the crystal chemical formula in atoms per formula unit (*a.p.f.u.*) in Table 2 is based on the assumption

that $Fe^{2+}/Fe^{3+}$ = 9:1, as deduced by the Mössbauer data (Table 7). In addition, the $^{57}Fe$ Mössbauer spectrum of our ferroaxinite shows unambiguously the occurrence of $Fe^{2+}$ and $Fe^{3+}$ in octahedral coordination only. The narrow width of the peaks suggests to rule out a potential multi-sites distribution of $Fe^{3+}$. In this light, it is highly likely that $Fe^{3+}$ populates the octahedral *Z1* site only, along with Al, according to the previous experimental findings (*e.g.*, Andreozzi et al. 2000a, 2000b, 2004; Zabinski et al. 2002; Filip et al. 2006). We tend to consider unlikely the assumption that $Fe^{3+}$ populates the tetrahedral sites, as previously reported by Pieczka and Kraczka (1994) and Fuchs et al. (1997) for samples of Polish and Norwegian axinites, respectively.

The neutron structure refinement of ferroaxinite of this study provides a structure model in general agreement with the experimental findings so far reported: site positions, bond distances and angles are comparable with those previously published (*e.g.*, Takéuchi et al. 1974; Swinnea et al. 1981; Belokoneva et al. 1997, 2001; Andreozzi et al. 2000a, 2000b, 2004; Filip et al. 2006). In our structure refinement, the tetrahedral *T1*, *T2*, *T3* and *T4* sites are fully occupied by Si, whereas the *T5* site is fully occupied by B. There is no evidence of Si at the *T5*, or Al or $Fe^{3+}$ at the *T1*-*T5* sites. The structural and chemical data of this study suggest that the amount of B in ferroaxinite is that expected from the ideal stoichiometry: 2 *a.p.f.u.* (for 32 O). The *T5* tetrahedron shows an average intra-tetrahedral bond distance of ~1.485 Å, with a difference between the longest and the shortest bond distance of about 0.1 Å (Table 6). In our refinement, the *X1* site is found to be fully populated and the *X2* mainly populated by Ca, and a low fraction of Mn is present at the *X2* site (Table 4). The octahedral *Y* site is mainly populated by Fe (*i.e.*, we expect $Fe^{2+}$, ~76%), and in minor fraction by Mn (~24%). The *Z1* site is almost fully occupied by Al (*i.e.*, ~95%), and only a minor fraction of Fe (we expect $Fe^{3+}$, ~5%) is present. The *Z2* site contains Al only.

The chemical formula deduced on the basis of the structure refinement is the following:

$^{X1,X2}(Ca_{3.98}Mn_{0.02})_{\Sigma 4}{}^{Y}(Mn_{0.48}Fe_{1.52})_{\Sigma 2}{}^{Z1,Z2}(Fe_{0.10}Al_{3.90})_{\Sigma 4}{}^{T1,T2,T3,T4}Si_8{}^{T5}B_2O_{30}(OH)_2$,

whereas that obtained by ICP-AES is:

$^{X1,X2}Ca_{4.03}{}^{Y}(Mn_{0.42}Mg_{0.23}Fe^{2+}_{1.39})_{\Sigma 2.04}{}^{Z1,Z2}(Fe^{3+}_{0.15}Al_{3.55}Ti_{0.12})_{\Sigma 3.82}{}^{T1;T2,T3,T4}(Ti_{0.03}Si_{7.97})_{\Sigma 8}{}^{T5}B_{1.96}O_{30}(OH)_{2.18}$.

As Mg and Ti were not considered in the neutron structure refinement, a comparison between the results of the refinement and the chemical analysis should be done on the basis of the number of electrons per site:

(SCND) $^{X1,X2}[80.1e\text{-}]^{Y,Z1,Z2}[104.8e\text{-}]^{T1,T2,T3,T4}[112.0e\text{-}]^{T5}[10.0e\text{-}]O_{30}(OH)_2$,

(ICP-AES) $^{X1,X2}[80.6e\text{-}]^{Y,Z1,Z2}[102.2e\text{-}]^{T1,T2,T3,T4}[112.2e\text{-}]^{T5}[9.8e\text{-}]O_{30}(OH)_{2.18}$,

showing a very good agreement.

For the first time, the neutron diffraction data allowed an unambiguous localization of the H site, which forms a hydroxyl group with the oxygen atom at the *O16* site as *donor* (Tables 4 and 6). The

H-bonding scheme in the axinite structure is fully shown by Fig. 4: the *O16-H* distance (corrected for riding motion effect, Busing and Levy 1964) is 0.991(1) Å and an asymmetric bifurcated bonding configuration occurs, with *O5* and *O13* as *acceptors* (Table 6):

- *O16*···*O5* = 3.096(1) Å, *H*···*O5* = 2.450(1) Å and *O16-H*···*O5* = 123.9(1)°;
- *O16*···*O13* = 2.777(1) Å, *H*···*O13* = 1.914(1) Å and *O16-H*···*O13* = 146.9(1)°.

The *O16-H*···*O5* bond is weaker than the *O16-H*···*O13* one, as suggested by the refined distances and angles. Other potential H-bonds, with *O5'* (*i.e.*, *O16*···*O5* = 2.786(1) Å and *O16-H*···*O5* = 83(1)°), *O14* (*i.e.*, *O16*···*O14* = 2.796(1) Å and *O16-H*···*O14* = 80.1(1), and *O16* (*i.e.*, *O16*···*O16* = 3.634(1) Å and *O16-H*···*O16* = 134.0(1)°) as *acceptors*, can be ruled out as energetically unfavourable.

A clue of the H-bonding configuration in axinite structure was first reported by Takèuchi (1975), on the basis of the X-ray and IR data available at that time (Beran 1971; Takèuchi et al. 1974). A more recent study by Filip et al. (2006) based on FTIR and X-ray data, in which the H-bonding scheme in axinite is described, reports: *i)* an intense IR-active band (broad and asymmetric) with the maximus at ~3382 $cm^{-1}$, along with a very low-intensity band at ~3485 $cm^{-1}$, and *ii)* a hydrogen bonding scheme based on *O16-H* ~ 0.83 Å, *O16*···*O13* ~ 2.78 Å and *O16-H*···*O13* ~ 151°. The authors considered a H-bond configuration based on one acceptor only (*i.e.*, *O13*) and deduced from the distance–frequency correlation of Libowitzky (1999) the expected $O_{donor}$···$O_{acceptor}$ distance of 2.8 Å, in good agreement with the refined $O_{donor}$···$O_{acceptor}$ distance (Filip et al. 2006). The low-intensity band at ~3485 $cm^{-1}$ was ascribed to *O16* as potential acceptor, with *O16*···*O16* ~ 3.11 Å and *O16-H*···*O16* ~ 126°. The neutron structure refinement of this study shows that the H-bonding scheme in axinite structure is actually more complex: the broad and asymmetric IR-band with the maximus at ~3382 $cm^{-1}$ might represent the convolution of at least two different contributes, according to the bifurcated H-bonding configuration here found. The low-intensity IR-band at ~3485 $cm^{-1}$ can accordingly be due to energetically weaker H-bonds, with *O5'*, *O14* and *O16* as *acceptors*, in agreement with the experimental findings of this study.

A careful inspection of the displacement parameters reported in Table 5 shows a pronounced magnitude of the displacement ellipsoid of H, though with a not drastic anisotropy. However, the difference-Fourier map of the nuclear density, phased without the *H* site, shows no evidence of site split (Fig. 2). Even the *O4* and *O11* sites are described with a slightly pronounced anisotropic displacement ellipsoids, which likely reflect their bonding configurations and the multi-element population of the octahedral sites, with a resulting local difference in the cation-O bonding distances.

## Acknowledgements

The authors acknowledge the Neutronenquelle Heinz Maier-Leibnitz Zentrum (MLZ) in Garching, Germany, for the allocation of neutron beam time at the single crystal diffractometer HEIDI operated by RWTH Aachen University and Jülich Centre for Neutron Science (JARA-FIT cooperation). GDG and AP acknowledge the financial support of the Italian Ministry of Education (MIUR) – PRIN 2011, ref. 2010EARRRZ. G. Andreozzi and an anonymous reviewer are thanked.

## References

Andreozzi GB, Ottolini L, Lucchesi S, Graziani G, Russo U (2000a) Crystal chemistry of the axinite-group minerals: A multi-analytical approach. Am Mineral 85:698–706.

Andreozzi GB, Lucchesi S, Graziani G (2000b) Structural study of magnesioaxinite and its crystal-chemical relations with axinite-group minerals. Eur J Mineral 12:1185–1194.

Andreozzi GB, Lucchesi S, Graziani G, Russo U (2004) Site distribution of $Fe^{2+}$ and $Fe^{3+}$ in the axinite mineral group: new crystal-chemical formula. Am Mineral 89:1763-1771.

Belokoneva EL, Pletnev PA, Spiridonov EM (1997) Crystal structure of low-manganese tinzenite (severginite). Crystallogr Rep 42:1010–1013.

Belokoneva EL, Goryunova AN, Pletnev PA, Spiridonov EM (2001) Crystal structure of high-manganese tinzenite from the Falotta deposit in Switzerland. Crystallogr Rep 46:30-32.

Beran A (1971) Messung des Ultrarot-Pleochroismus von Mineralen. XIII. Der Pleochroismus der OH-Streckfrequenz in Axinit. Tschermaks Min Petr Mitt 16:281-286.

Blissett AH (1962) Zeehan. One Mile Geological Map Series. Geological Survey of Tasmania Explanatory Report, sheet K'55-5-50. Department of Mines, Tasmania, 272 p.

Busing WR, Levy HA (1964) The effect of thermal motion on the estimation of bond lengths from diffraction measurements. Acta Crystallogr 17:142-146.

Farrugia LJ (1999) WinGX suite for small-molecule single-crystal crystallography. J Appl Crystallogr 32:837-838.

Filip J, Kolitsch U, Novak M, Schneeweiss O (2006) The crystal structure of near-end-member ferroaxinite from an iron-contaminated pegmatite at Malešov, Czech Republic. Can Mineral 44:1159-1170.

Filip J, Dachs E, Tuček J, Novák M, Bezdička P (2008) Low-temperature calorimetric and magnetic data for natural end-members of the axinite group. Am Mineral 93:548-557.

Fuchs Y, Linares J, Robert JL (1997) Mössbauer and FTIR characterization of a ferro-axinite. Hyperfine Interact 108:527–533.

Gatta GD, Vignola P, McIntyre GJ, Diella V (2010) On the crystal chemistry of londonite [(Cs,K,Rb)$Al_4Be_5B_{11}O_{28}$]: a single-crystal neutron diffraction study at 300 and 20 K. Am Mineral 95:1467–1472.

Gatta GD, McIntyre GJ, Bromiley G, Guastoni A, Nestola F (2012a) A single-crystal neutron diffraction study of hambergite, $Be_2BO_3$(OH,F). Am Mineral 97:1891–1897.

Gatta GD, Danisi RM, Adamo I, Meven M, Diella V (2012b) A single-crystal neutron and X-ray diffraction study of elbaite. Phys Chem Minerals 39:577–588.

Gatta GD, Bosi F, McIntyre GJ, Skogby H (2014a) First accurate location of two proton sites in tourmaline: A single-crystal neutron diffraction study of oxy-dravite. Min Mag 78:681-692.

Gatta GD, Nénert G, Guastella G, Lotti P, Guastoni A, Rizzato S (2014b) A single-crystal neutron and X-ray diffraction study of a Li,Be-bearing brittle mica. Min Mag 78:55–72.

Grew ES (1996) Borosilicates (exclusive of tourmaline) and boron in rock-forming minerals in metamorphic environments. Rev Mineral 33:387–502.

Ito T, Takéuchi Y (1952) The crystal structure of axinite. Acta Crystallogr 5:202-208.

Ito T, Takéuchi Y, Ozawa T, Ariki T, Zoltai T, Finnet SS (1969) The crystal structure of axinite revised. Proc Jap Acad 45:490-494.

Larson AC (1967) Inclusion of secondary extinction in least-squares calculations. Acta Crystallogr 23:664 – 665.

Libowitzky E (1999) Correlation of O–H stretching frequencies and O–H...O hydrogen bond lengths in minerals. Monatsh Chem 130:1047-1059.

Lumpkin GR, Ribbe PH (1979) Chemistry and physical properties of axinites. Am Mineral 64:635–645.

Novák M, Filip J (2002) Ferroan magnesioaxinite from hydrothermal veins at Lazany, Brno Batholith, Czech Republic. Neues Jahrb Mineral Monatsh 385-399.

Petterd WF (1910) The Minerals of Tasmania. Papers and Proceedings of the Royal Society of Tasmania for 1910, 221 p.

Pieczka A, Kraczka J (1994) Crystal chemistry of $Fe^{2+}$-axinite from Strzegom. Mineralogica Polonica 25:43–49.

Pouchou JL, Pichoir F (1985) "PAP" correction procedure for improved quantitative microanalysis. In: JT Armstrong, Ed, Microbeam Analysis. San Francisco Press, 104-106.

Pringle IJ, Kawachi Y (1980) Axinite mineral group in low-grade regionally metamorphosed rocks in southern New Zealand. Am Mineral 65:1119–1129.

Rancourt DG, Ping JY (1991) Voigt-based methods for arbitrary-shape static hyperfine parameter distributions in Mössbauer spectroscopy. Nucl Instr Meth Phys Res B 58:85-97.

Sanero E, Gottardi G (1968) Nomenclature and crystal chemistry of axinites. Am Mineral 53:1407–1411.

Sears VF (1986) Neutron Scattering Lengths and Cross-Sections. In K. Sköld and D.L. Price, Eds., Neutron Scattering, Methods of Experimental Physics, Vol. 23A, p. 521-550. Academic Press, New York.

Sheldrick GM (1997) SHELX-97. Programs for crystal structure determination and refinement. University of Göttingen, Germany.

Sheldrick GM (2008) A short history of SHELX. Acta Cryst A64:112-122.

Swinnea JS, Steinfink H, Rendon-Diaz Miron LE, Enciso de La Vega S (1981) The crystal structure of a Mexican axinite. Am Mineral 66:428–431.

Takéuchi Y, Ozawa Y, Ito T, Araki T, Zoltai T, Finney JJ (1974) The B2Si8O30 groups of tetrahedra in axinite and comments on deformation of Si tetrahedra in silicates. Z Kristallogr 140:289–312.

Zabinski W, Pieczka A, Kraczka J (2002) A Mössbauer study of two axinites from Poland. Mineralogica Polonica 33:27–33.

Table 1. Representative composition of the ferroaxinite from Colebrook Hill, based on EPMA-WDS analysis (average of 20 data points). The chemical formula (calculated on the basis of 32 oxygen atoms and with $Fe^{2+}/Fe^{3+}$ = 9:1, as suggested by the Mössbauer data) is the following:
$^{X1,X2}(Ca_{3.86}Mn_{0.07})_{\Sigma 3.93}{}^{Y}(Mn_{0.32}Mg_{0.09}Fe^{2+}_{1.45}Fe^{3+}_{0.14})_{\Sigma 2.00}{}^{Z1,Z2}Al_{4.00}{}^{T1,T2,T3,T4}(Al_{0.04}Ti_{0.01}Si_{7.94})_{\Sigma 7.99}{}^{T5}B_2O_{30}(OH)_{2.18}$

| | wt% | *e.s.d.* | | *a.p.f.u.* |
|---|---|---|---|---|
| MgO | 0.33 | 0.08 | Mg | 0.09 |
| CaO | 19.10 | 0.3 | Ca | 3.86 |
| MnO | 2.43 | 0.1 | $Mn^{2+}$ | 0.39 |
| FeO | 9.16 | 0.2 | $Fe^{2+}$ | 1.45 |
| $Fe_2O_3$ | 0.89 | 0.2 | $Fe^{3+}$ | 0.14 |
| $B_2O_3$ | 6.11 | 0.15 | $B^{3+}$ | 2.00 |
| $Al_2O_3$ | 18.15 | 0.2 | Al | 4.04 |
| $SiO_2$ | 42.06 | 0.8 | Si | 7.94 |
| $TiO_2$ | 0.04 | 0.02 | $Ti^{4+}$ | 0.01 |
| $H_2O$* | 1.73 | | $OH^-$ | 2.18 |
| TOTAL | 100.00 | | | |

* calculated by difference to 100 wt%; $B_2O_3$ calculated from the ideal stoichiometry.

Table 2. Chemical composition of the ferroaxinite sample based on ICP-AES analysis. The chemical formula (calculated on the basis of 32 oxygen atoms and with $Fe^{2+}/Fe^{3+}$ = 9:1, as suggested by the Mössbauer data) is the following:
$^{X1,X2}Ca_{4.03}{}^{Y}(Mn_{0.42}Mg_{0.23}Fe^{2+}_{1.39})_{\Sigma 2.04}{}^{Z1,Z2}(Fe^{3+}_{0.15}Al_{3.55}Ti_{0.12})_{\Sigma 3.82}{}^{T1;T2,T3,T4}(Ti_{0.03}Si_{7.97})_{\Sigma 8.00}{}^{T5}B_{1.96}O_{30}(OH)_{2.18}$

| Oxides | wt% | *e.s.d.* | λ ICP/AES (nm) | Alkaline fusion - ICP/AES | Microwave assisted acid digestion - ICP/AES | wet method |
|---|---|---|---|---|---|---|
| $SiO_2$ | 41.9 | 0.7 | 251.611 | x | | (1) |
| FeO | 9.71 | 0.3 | 238.204 | x | x | |
| MnO | 2.62 | 0.15 | 257.610 | x | x | |
| $Cr_2O_3$ | 0.09 | n.d. | 267.716 | x | x | |
| $TiO_2$ | 1.07 | 0.25 | 334.940 | x | x | |
| $Al_2O_3$ | 16.0 | 0.5 | 396.153 | x | x | (2) |
| CaO | 19.8 | 0.6 | 317.933 | x | x | |
| MgO | 0.81 | 0.20 | 285.213 | x | x | |
| $B_2O_3$ | 5.97 | 0.30 | 208.957<br>249.677 | x | | |
| $K_2O$ | 0.03 | n.d. | 766.490 | x | x | |
| ZnO | 0.06 | n.d. | 206.200 | x | x | |
| SrO | 0.06 | n.d. | 407.771 | x | x | |
| $P_2O_5$ | 0.05 | n.d. | 213.617 | x | x | |
| $H_2O$* | 1.83 | | | | | |
| Total | 100.00 | | | | | |

(1) gravimetric method; (2) CyDTA-Zinc back titration method; * by difference to 100 wt%; $Li_2O$, BeO and $Na_2O$ contents were below the detection limit.

Table 3. Data pertaining to the neutron data collection and structure refinements of ferroaxinite.

| | |
|---|---|
| $T$ (K) | 293 |
| Crystal size (mm) | 3.2 x 3.1 x 2.5 |
| Neutron radiation | Constant wavelengths:<br>*A*: λ=1.170(2) Å,<br>*B*: λ=0.7925(5) Å |
| Reference formula | $Ca_4(Mn,Fe)_2Al_4B_2Si_8O_{30}(OH)_2$ |
| $Z$ | 1 |
| Scan details: | |
| λ, time/step, collimation, range, type, steps ($u$, $v$, $q$) | *A*: 1 – 6 s, 60',<br>6.5°<2θ<80°, ω-scan, 41 steps (17.4, -66, 79)<br>80°< 2θ<100°, ω-θ-scan, 31 steps (18, -65, 85)<br>100°<2θ<124°, ω-2θ scan, 25 steps (15, 0, 0)<br>*B*: 2 – 8 s, 60',<br>75°<2θ<90°, ω-θ scan, 35 steps (12.25, 0, 0) |
| Space Group | *P*-1 |
| $a$ (Å) | 7.1629(2) |
| $b$ (Å) | 9.2019(3) |
| $c$ (Å) | 8.9608(3) |
| α (°) | 91.792(2) |
| β (°) | 98.227(3) |
| γ (°) | 77.307(3) |
| $d_{min}$ (Å) | 0.56 |
| $V$ (Å$^3$) | 570.26(3) |
| $h_{min}/h_{max}$, $k_{min}/k_{max}$, $l_{min}/l_{max}$ | -12/+12, -16/+16, -16/+16 |
| $d_{min}$ (Å) | 0.56 |
| Measured reflections | 6525 (5724 + 801) |
| Reflections with $F_O > 4\sigma(F_O)$ | 5440 |
| $R_{Friedel}$, $R_\sigma$ | 0.0271, 0.0445 |
| N. of refined parameters | 251 |
| $R_1$, observed reflections | 0.0320 |
| $R_1$, all reflections | 0.0486 |
| w$R^2$, all reflections | 0.0611 |
| GoF | 1.398 |
| Extinction coefficient | 0.0189(9) |
| Residuals (fm/ Å$^3$) | -0.86 / +0.87 |

$R_{int}=\Sigma|F_{obs}^2-F_{obs}^2{}_{(mean)}|/\Sigma[F_{obs}^2]$, based on the Friedel pairs; $R_1=\Sigma(||F_{obs}|-|F_{calc}||)/\Sigma|F_{obs}|$;
$wR_2=[\Sigma[w(F^2_{obs}-F^2_{calc})^2]/\Sigma[w(F^2_{obs})^2]]^{0.5}$, $w=1/[\sigma^2(F_{obs}^2)+(0.01*P)^2]$, $P=(\mathrm{Max}(F_{obs}^2,0)+2*F_{calc}^2)/3$.
Unit-cell parameters based on single-crystal X-ray data (1980 reflections, CCD). Isotropic extinction coefficient based on the Larson's formalism (Larson 1967), as implemented in SHELIX97;
scan width = $(u + v*\tan\theta + q*\tan^2\theta)^{0.5}$.

Table 4. Fractional atomic coordinates and displacement parameters (Å$^2$) of ferroaxinite based on the neutron structure refinement. $U_{eq}$ is defined as one third of the trace of the orthogonalized $U_{ij}$ tensor.

| *Site* | *s.o.f.* | *x/a* | *y/b* | *z/c* | $U_{eq}$ |
|---|---|---|---|---|---|
| *T1* | Si 1 | 0.21088(10) | 0.45011(8) | 0.23474(9) | 0.0051(1) |
| *T2* | Si 1 | 0.21938(10) | 0.27470(8) | 0.52352(8) | 0.0045(1) |
| *T3* | Si 1 | 0.69910(10) | 0.25627(8) | 0.01159(8) | 0.0051(1) |
| *T4* | Si 1 | 0.64123(10) | 0.01939(8) | 0.23025(8) | 0.0046(1) |
| *T5* | B 1 | 0.46163(8) | 0.63455(6) | 0.28663(6) | 0.0041(1) |
| *X1* | Ca 1 | 0.74635(10) | 0.34819(8) | 0.39532(8) | 0.0083(2) |
| *X2* | Ca 0.990(2), Mn 0.010(2) | 0.18262(10) | 0.10048(8) | 0.08406(8) | 0.0088(2) |
| *Y* | Mn 0.241(1), Fe 0.759(1) | 0.76734(7) | 0.59191(6) | 0.11238(6) | 0.0090(1) |
| *Z1* | Al 0.947(3), Fe 0.053(3) | 0.05229(11) | 0.80096(9) | 0.25382(9) | 0.0047(2) |
| *Z2* | Al 1 | 0.35219(12) | 0.93630(10) | 0.42114(10) | 0.0044(1) |
| *O1* | O 1 | 0.05439(8) | 0.60314(6) | 0.18978(6) | 0.0073(1) |
| *O2* | O 1 | 0.23147(8) | 0.33836(7) | 0.09633(7) | 0.0098(1) |
| *O3* | O 1 | 0.41890(7) | 0.48708(6) | 0.31239(7) | 0.0074(1) |
| *O4* | O 1 | 0.13602(8) | 0.37268(7) | 0.37032(7) | 0.0107(1) |
| *O5* | O 1 | 0.02202(7) | 0.24227(6) | 0.56404(6) | 0.0072(1) |
| *O6* | O 1 | 0.32690(7) | 0.37996(6) | 0.64496(6) | 0.0068(1) |
| *O7* | O 1 | 0.38066(7) | 0.12749(6) | 0.49608(6) | 0.0060(1) |
| *O8* | O 1 | 0.53638(8) | 0.34365(6) | 0.87694(6) | 0.0074(1) |
| *O9* | O 1 | 0.87613(7) | 0.15473(6) | 0.93409(6) | 0.0067(1) |
| *O10* | O 1 | 0.76849(8) | 0.36671(7) | 0.13903(7) | 0.0093(1) |
| *O11* | O 1 | 0.60328(8) | 0.13526(7) | 0.08758(7) | 0.0099(1) |
| *O12* | O 1 | 0.43639(7) | 0.98157(6) | 0.24383(6) | 0.0066(1) |
| *O13* | O 1 | 0.72103(8) | 0.09950(6) | 0.38433(6) | 0.0067(1) |
| *O14* | O 1 | 0.79380(7) | 0.87452(6) | 0.17720(6) | 0.0077(1) |
| *O15* | O 1 | 0.32548(7) | 0.74608(6) | 0.35443(6) | 0.0055(1) |
| *O16* | O 1 | 0.09649(7) | 0.99606(6) | 0.32272(6) | 0.0064(1) |
| *H* | H 1 | -0.00645(16) | 1.04412(14) | 0.37875(14) | 0.0216(2) |

Table 5. Refined displacement parameters (Å$^2$) in the expression: $-2\pi^2[(ha^*)^2U_{11} + \ldots + 2hka^*b^*U_{12} + \ldots + 2klb^*c^*U_{23}]$.

| | $U_{11}$ | $U_{22}$ | $U_{33}$ | $U_{23}$ | $U_{13}$ | $U_{12}$ |
|---|---|---|---|---|---|---|
| *T1* | 0.0055(3) | 0.0053(3) | 0.0046(3) | 0.0011(2) | 0.0005(2) | -0.0013(2) |
| *T2* | 0.0040(2) | 0.0049(3) | 0.0047(3) | 0.0010(2) | 0.0006(2) | -0.0012(2) |
| *T3* | 0.0058(3) | 0.0051(3) | 0.0042(3) | 0.0009(2) | 0.0013(2) | -0.0003(2) |
| *T4* | 0.0050(3) | 0.0062(3) | 0.0029(3) | 0.0007(2) | 0.0009(2) | -0.0017(2) |
| *T4* | 0.0041(2) | 0.0045(2) | 0.0039(2) | 0.0002(2) | 0.0012(2) | -0.0006(2) |
| *X1* | 0.0097(3) | 0.0062(3) | 0.0081(3) | 0.0018(2) | -0.0005(2) | -0.0007(2) |
| *X2* | 0.0101(3) | 0.0090(3) | 0.0070(3) | 0.0021(2) | -0.0023(2) | -0.0037(2) |
| *Y* | 0.0062(2) | 0.0130(2) | 0.0081(3) | 0.0036(2) | 0.0008(2) | -0.0022(2) |
| *Z1* | 0.0048(3) | 0.0050(3) | 0.0045(4) | 0.0004(3) | 0.0008(2) | -0.0012(2) |
| *Z2* | 0.0043(3) | 0.0049(3) | 0.0040(4) | -0.0005(3) | 0.0007(2) | -0.0009(2) |
| *O1* | 0.0072(2) | 0.0057(2) | 0.0084(2) | 0.0012(2) | 0.0001(2) | -0.0005(2) |
| *O2* | 0.0127(2) | 0.0082(2) | 0.0082(2) | -0.0019(2) | 0.0019(2) | -0.0020(2) |
| *O3* | 0.0060(2) | 0.0064(2) | 0.0098(2) | 0.0017(2) | -0.0002(2) | -0.0020(2) |
| *O4* | 0.0096(2) | 0.0146(2) | 0.0085(2) | 0.0072(2) | -0.0002(2) | -0.0040(2) |
| *O5* | 0.0055(2) | 0.0113(2) | 0.0054(2) | 0.0017(2) | 0.0012(2) | -0.0026(2) |
| *O6* | 0.0055(2) | 0.0071(2) | 0.0076(2) | -0.0018(2) | -0.0001(2) | -0.0018(2) |
| *O7* | 0.0049(2) | 0.0055(2) | 0.0074(2) | -0.0013(2) | 0.0004(2) | -0.0010(2) |
| *O8* | 0.0076(2) | 0.0091(2) | 0.0046(2) | 0.0020(2) | 0.0013(2) | 0.0007(2) |
| *O9* | 0.0062(2) | 0.0072(2) | 0.0066(2) | 0.0004(2) | 0.0020(2) | -0.0004(2) |
| *O10* | 0.0117(2) | 0.0100(2) | 0.0064(2) | -0.0014(2) | 0.0007(2) | -0.0031(2) |
| *O11* | 0.0113(2) | 0.0117(2) | 0.0079(2) | 0.0050(2) | 0.0011(2) | -0.0039(2) |
| *O12* | 0.0060(2) | 0.0097(2) | 0.0051(2) | 0.0006(2) | 0.0014(2) | -0.0033(2) |
| *O13* | 0.0078(2) | 0.0085(2) | 0.0049(2) | -0.0011(2) | 0.0018(2) | -0.0036(2) |
| *O14* | 0.0055(2) | 0.0093(2) | 0.0073(2) | -0.0010(2) | 0.0004(2) | 0.0003(2) |
| *O15* | 0.0055(2) | 0.0056(2) | 0.0053(2) | -0.0007(2) | 0.0015(2) | -0.0011(2) |
| *O16* | 0.0054(2) | 0.0072(2) | 0.0066(2) | -0.0004(2) | 0.0009(2) | -0.0012(2) |
| *H* | 0.0186(5) | 0.0223(5) | 0.0239(6) | -0.0038(4) | 0.0101(4) | -0.0004(4) |

Table 6. Relevant bond distances (Å) and angles (°) based on the neutron structure refinement of ferroaxinite.

| | | | | | |
|---|---|---|---|---|---|
| *T1-* | O2 | 1.5885(10) | *X2-* | O12 | 2.2428(9) |
| | O1 | 1.6169(9) | | O2 | 2.2883(10) |
| | O4 | 1.6369(9) | | O9 | 2.3645(9) |
| | O3 | 1.6527(9) | | O14 | 2.3929(9) |
| | Av. | 1.6238 | | O9 | 2.4718(9) |
| | | | | O16 | 2.5776(9) |
| *T2-* | O5 | 1.5995(9) | | [O11 | 2.9030(10)] |
| | O7 | 1.6133(9) | | [O11 | 3.0949(9)] |
| | O4 | 1.6311(9) | | | |
| | O6 | 1.6546(10) | | | |
| | Av. | 1.6246 | *Y-* | O2 | 1.9979(8) |
| | | | | O10 | 2.0915(8) |
| *T3-* | O10 | 1.6034(10) | | O1 | 2.0976(8) |
| | O9 | 1.6291(9) | | O8 | 2.1407(7) |
| | O11 | 1.6406(9) | | O6 | 2.3577(8) |
| | O8 | 1.6453(9) | | O14 | 2.6880(8) |
| | Av. | 1.6296 | | | |
| | | | | | |
| *T4-* | O12 | 1.6021(9) | *Z1-* | O14 | 1.8634(9) |
| | O14 | 1.6328(9) | | O5 | 1.8675(10) |
| | O13 | 1.6347(9) | | O1 | 1.8890(10) |
| | O11 | 1.6443(9) | | O9 | 1.9096(10) |
| | Av. | 1.6285 | | O16 | 1.9568(10) |
| | | | | O15 | 1.9965(9) |
| *T5-* | O15 | 1.4367(8) | | | |
| | O3 | 1.4868(8) | | | |
| | O8 | 1.4882(8) | *Z2-* | O12 | 1.8675(10) |
| | O6 | 1.5292(8) | | O15 | 1.8727(11) |
| | Av. | 1.4852 | | O16 | 1.8868(10) |
| | | | | O7 | 1.9058(11) |
| *X1-* | O13 | 2.3330(9) | | O7 | 1.9194(10) |
| | O10 | 2.3386(10) | | O13 | 1.9482(10) |
| | O5 | 2.3509(9) | | | |
| | O3 | 2.4352(9) | | | |
| | O6 | 2.4675(9) | | | |
| | O15 | 2.5872(9) | | | |
| | [O4 | 2.8897(9)] | | | |
| | | | | | |
| *O16-H* | | 0.970(1) | | | |
| *O16-H** | | 0.991(1) | | | |
| *O16···O5* | | 3.096(1) | | | |
| *H···O5* | | 2.450(1) | | | |
| *O16-H···O5* | | 123.9(1) | | | |
| | | | | | |
| *O16···O13* | | 2.777(1) | | | |
| *H···O13* | | 1.914(1) | | | |
| *O16-H···O13* | | 146.9(1) | | | |

*Corrected for riding motion effect following Busing and Levy (1964).

Table 7. $^{57}$Fe Mössbauer parameters of ferroaxinite.

| IS (mm/s) | QS (mm/s) | FWHM (mm/s) | Area (%) | Site assignment |
|---|---|---|---|---|
| 1.140(5) | 2.089(5) | 0.302(6) | 89.7(8) | $Fe^{2+}$ |
| 0.378(6) | 0.385(8) | 0.286(5) | 10.3(9) | $Fe^{3+}$ |

IS = isomer shift, QS = quadrupole splitting with respect to α-iron at room temperature, FWHM = full width at half maximum.

Figure 1. The crystal structure of ferroaxinite viewed down [100], [010], and [001], based on the neutron structure refinement of this study. An additional clinographic view shows the sequence of alternating sheets of tetrahedra and octahedra, which form the structure of axinite. Atomic displacement probability factor: 50%.

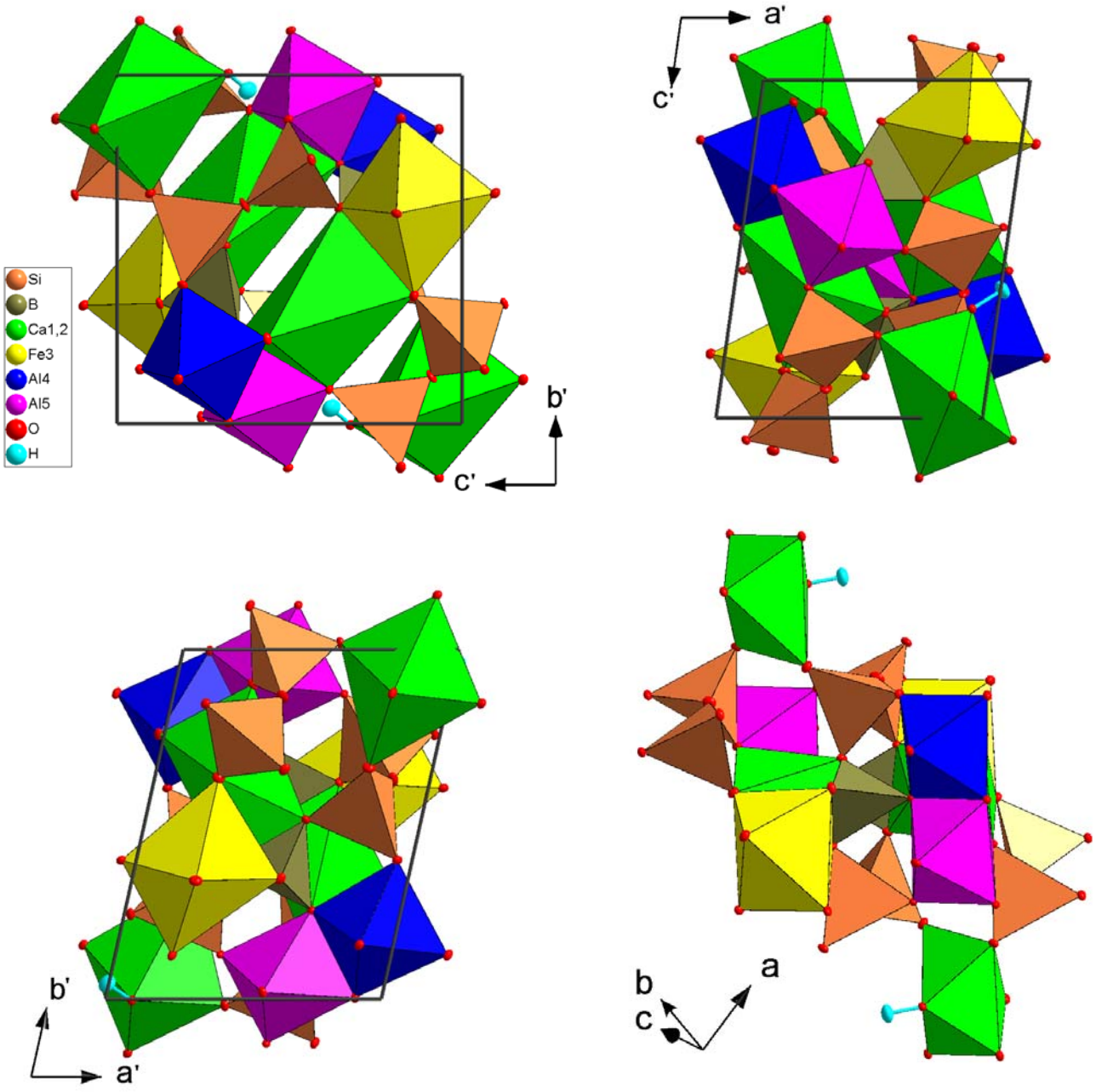

Figure 2. Difference-Fourier maps of the nuclear density (fm/Å$^3$) of ferroaxinite structure at $z \sim 0.38$, phased without the H site [section parallel to (001)].

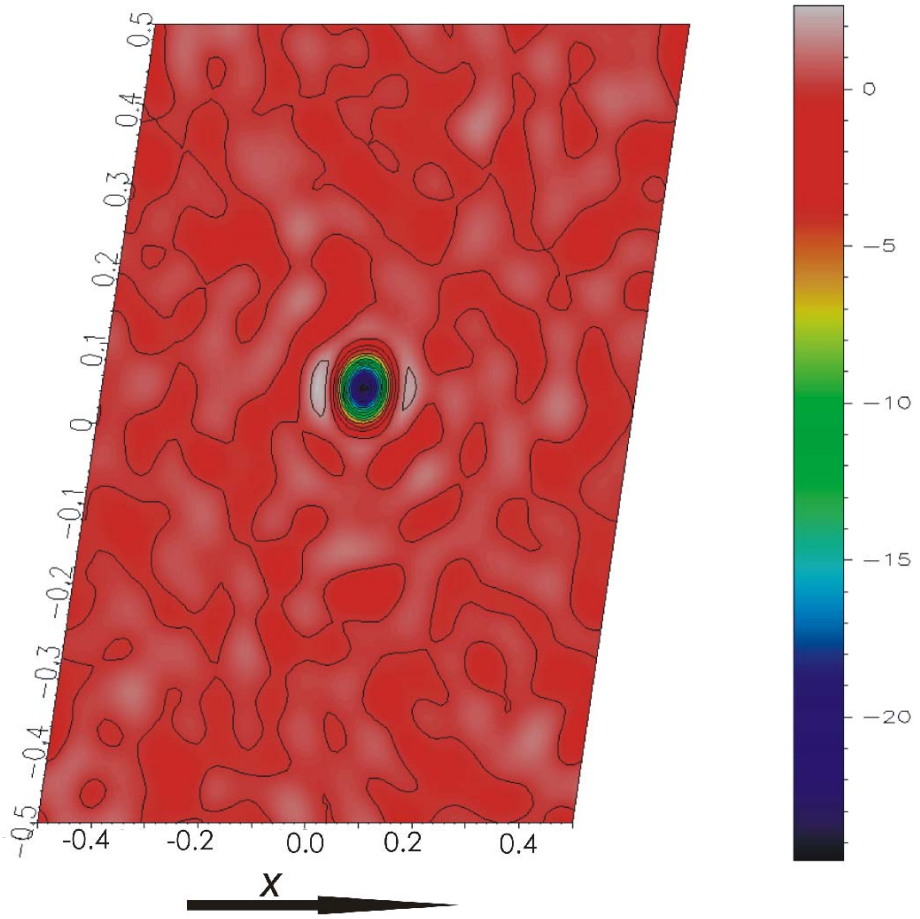

Figure 3. $^{57}$Fe Mössbauer spectrum of ferroaxinite at room temperature.

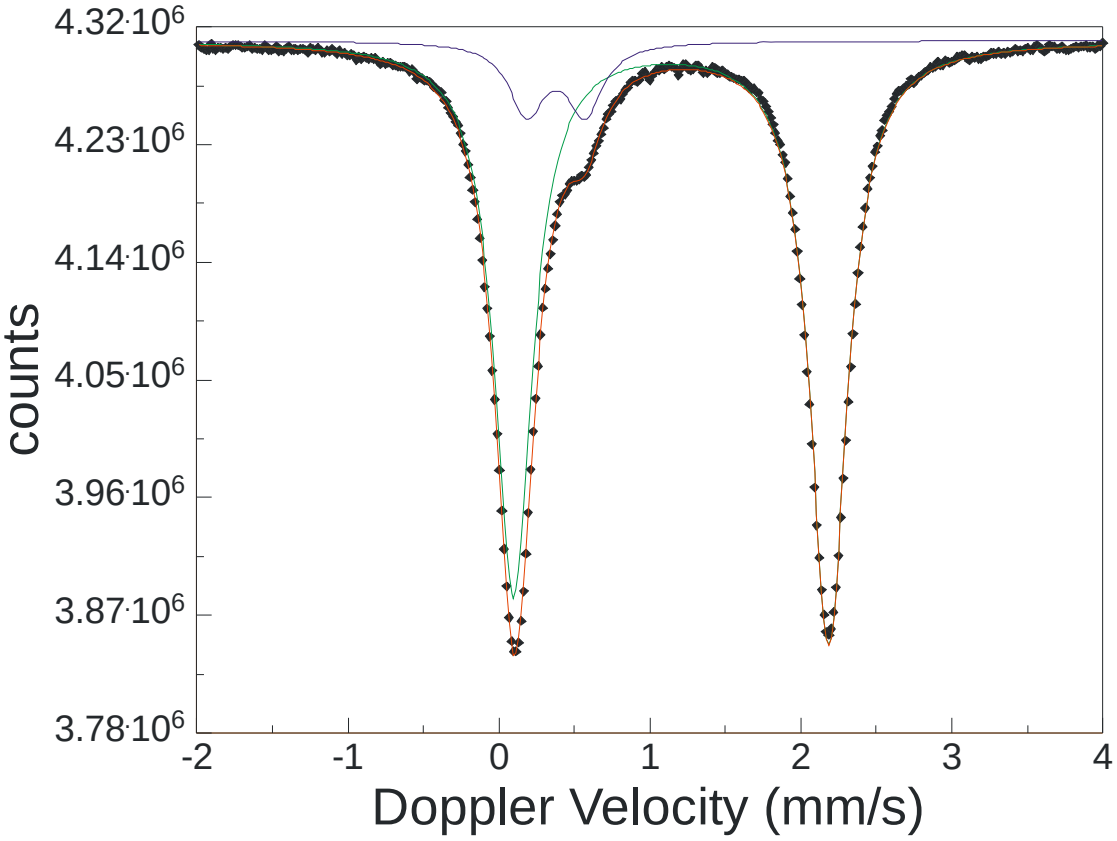

Figure 4. The H-bonding scheme (with a bi-furcated configuration) in axinite structure based on the neutron structure refinement of this study. Atomic displacement probability factor: 50%.